Hindawi
Journal of Nanomaterials
Volume 2020, Article ID 8305871, 13 pages
https://doi.org/10.1155/2020/8305871

Research Article

Synthesis and Characterization of Hierarchical Mesoporous-Macroporous TiO_2-ZrO_2 Nanocomposite Scaffolds for Cancellous Bone Tissue Engineering Applications

Shima Mahtabian,[1] **Zahra Yahay**,[1] **Seyed Mehdi Mirhadi**,[1] **and Fariborz Tavangarian**[2]

[1]*Department of Materials Engineering, Shahreza Branch, Islamic Azad University, 86145-311 Shahreza, Isfahan, Iran*
[2]*Mechanical Engineering Program, School of Science, Engineering and Technology, Pennsylvania State University, Harrisburg, Middletown, PA 17057, USA*

Correspondence should be addressed to Fariborz Tavangarian; fut16@psu.edu

Received 30 July 2020; Revised 31 August 2020; Accepted 17 September 2020; Published 6 October 2020

Academic Editor: Nicholas Dunne

Bone tissue engineering has been introduced several decades ago as a substitute for traditional grafting techniques to treat bone defects using engineered materials. The main goal in bone tissue engineering is to introduce materials and structures which can mimic the function of bone to restore the damaged tissue and promote cell restoration and proliferation. Titania and zirconia are well-known bioceramics which have been widely used in tissue engineering applications due to their unsurpassed characteristics. In this study, hierarchical meso/macroporous titania-zirconia (TiO_2-ZrO_2) nanocomposite scaffolds have been synthesized and evaluated for bone tissue engineering applications. The scaffolds were produced using the evaporation-induced self-assembly (EISA) technique along with the foamy method. To characterize the samples, X-ray diffraction (XRD), scanning electron microscopy (SEM), energy-dispersive X-ray spectroscopy (EDS), simultaneous thermal analysis (STA), and Brunauer-Emmett-Teller (BET) analysis were performed. The results showed that TiO_2-ZrO_2 scaffolds can be produced after sintering the samples at 550°C for 2 h. Among samples with different weight percentages of zirconia and titania, the sample containing 13 wt.% zirconia was considered as the optimum sample due to its structural integrity. This scaffold had pore size, pore wall size, and mesopores in the range of $185 \pm 66\,\mu$m, $15 \pm 4\,\mu$m, and 7-13 nm, respectively. The specific surface area obtained from the BET theory, total volume, and mean diameter of pores of this sample was 13.627 m^2g^{1-}, 0.03788 cm^3g^{-1}, and 11 nm, respectively. The results showed that the produced scaffolds can be considered as the promising candidates for cancellous bone regeneration.

1. Introduction

In recent decades, a great deal of effort and attention has been focused on designing scaffolds which are biologically, chemically, physically, mechanically, and structurally carefully matched to that of natural bone [1–23]. Although each type of bone tissue has specific requirements which must be met, there are some features in common that should be considered in designing bone scaffolds to present the exact function of host tissue [24, 25]. Generally, bone has a complex meso/macroporous hierarchical structure [24–29] with multisized interconnected pores [30, 31]. One of the main issues is to synthesize scaffolds with a hierarchical porous structure with pore interconnectivity to mimic the ECM of the host tissue. Different pore sizes play a remarkable role in enhancing cell viability and osteogenesis and finally in therapeutic effects for bone tissue engineering applications [32–36]. The macropore size of larger than 150 μm is required for cell accommodation and proliferation and also for vascularization [32, 37–42]. Mesopores with the size of 2-50 nm are also required to insert the nutrients and release the biological agents, to remove waste materials, and also to enhance the surface activity and bioactivity [37, 40–42].

Different techniques have been used to synthesize hierarchical structures including templating methods [43, 44], freeze-drying technique [45–47], and sol-gel method [48, 49]. In this study, the sol-gel method was utilized to synthesize the samples.

According to the literature, the sol-gel method is a facile way to synthesize metal oxide nanoparticles with high quality and purity at low temperatures. In this technique, precursors are dispersed in an aquatic or alcoholic environment at temperatures lower than 100°C. Through the hydrolysis and condensation, aggregation in the obtained colloidal solution which is called "sol" causes to make "gel" with a 3D network of M-O-M or M-OH-M units. Unlike other techniques such as the solid-state method, the sol-gel procedure requires low temperatures and very fine powders in which a homogeneous composition can be obtained. However, there are some disadvantages as well which should be considered such as a relatively high cost of initial precursors and the formation of cracks during the heat treatment cycles to remove the organic materials [50].

On the other hand, the evaporation-induced self-assembly technique (EISA) is a successful, simple, fast, and efficient method for the preparation of mesoporous metal oxides [51, 52]. The existence of hydrophobic and hydrophilic components in the surfactants causes the formation of micelle-like structures that are removed from the system by burning the hydrocarbon chains which leaves pores behind. This technique was first used to synthesize the silica mesoporous structure [53–55] and gradually was incorporated with the sol-gel method by using surfactants for other metal oxides [56]. Among many kinds of surfactants, the nonionic Pluronic F127 formed a well-organized mesopore structure [57].

TiO_2-ZrO_2 nanocomposite has been used in different applications. For example, Fu et al. [58] and Yu et al. [59] worked on its photocatalytic properties, individually. They reported that this nanocomposite shows better photocatalytic behavior compared to titania or zirconia, separately. The bioactivity of titania-zirconia nanocomposite has been studied by Marchi et al. [60]. The results showed an increase in apatite formation ability which indicates its good bioactivity in the biological environment. Also, this composite has been used as a 3D scaffold and coating. Tiainen et al. [61] investigated the mechanical properties of titania-zirconia nanocomposite scaffolds with different weight percentages of zirconia. The results showed that increasing the amount of zirconia in the composite decreased the mechanical strength of the scaffolds. Titania coating on its alloys is widely used in dental implants and hip prosthesis due to their excellent biocompatibility. According to the literature, TiO_2 has excellent biocompatibility, low toxicity, good corrosion resistance, and low density [62–64]. On the other hand, zirconia has several upsides over other bioceramics. Zirconia is bioinert in vivo and in vitro [65–67]. In vitro tests have shown that zirconia has lower toxicity than titanium oxide [68]. Additionally, cytotoxicity and carcinogenicity have not been reported [68]. Besides, it has good mechanical properties such as corrosion and abrasion resistance. Furthermore, it increases the crack self-healing potential of scaffolds by its transformation toughening mechanism [69, 70]. The strength of interfacial bonding between substrate and coating will be improved by the help of adding ZrO_2. Also, zirconia enhances apatite formation due to increasing the hydrophilicity of the substrate [71].

Figure 1: Schematic representation of the sol-gel method.

In the present study, for the first time, nanocomposite ZrO_2/TiO_2 scaffolds were produced using the EISA technique combined with the foamy method. Interconnected macropores were prepared by polyurethane (PU) (60 pores per inch (ppi)) sponge, and mesopores were made using Pluronic F127 surfactant by the help of a self-assembly technique in order to simulate the natural bone hierarchical porous structure. Structural features, chemical composition, and porosity features of the ZrO_2/TiO_2 nanocomposite scaffolds were evaluated. Furthermore, the formation mechanism of the produced scaffolds was evaluated as well.

2. Materials and Methods

2.1. Sample Preparation. In this study, the sol-gel technique was used to fabricate TiO_2-ZrO_2 nanocomposite scaffolds. A schematic representation of the sol-gel method is shown in Figure 1. To prepare the samples, titania and zirconia solutions were produced. Titania solution was prepared according to our previous study [72]. Briefly, 5 ml titanium (IV) butoxide ($C_{16}H_{36}O_4Ti$, 97%, Sigma-Aldrich) was added to 3.092 ml acetylacetone ($C_5H_8O_2$, 99.5%, Merck) and 125 ml absolute ethanol (C_2H_6O, 99.5%, Sigma-Aldrich). Next, a mixture of 2 gr Pluronic F127 (PF127, C_3H_3O $[C_2H_4O]_x$ $[C_3H_6O]_y[C_2H_4O]_zC_3H_3O_2$, 99.5%, Sigma-Aldrich) that was dissolved in 125 ml absolute ethanol (C_2H_6O, 99.5%, Sigma-Aldrich) and 6.67 ml hydrochloric acid (HCL, 38 wt.%, to adjust the pH solution to 4 as the zeta potential of the solution in order to disperse the particles and avoid coagulation) was gently added to the previous solution, stirred for 24 h with the speed of 1000 rpm at room temperature, and then aged for 48 h at a location with 40% humidity.

Table 1: Designation and specification of different samples.

Sample designation	TiO_2 content (wt.%)	ZrO_2 content (wt.%)	Solution type	Including foam	Including solution	Heat treatment
S_{13Zr}	87	13	A	✓	✓	✓
S_{26Zr}	74	26	B	✓	✓	✓
S_{50Zr}	50	50	C	✓	✓	✓
S_{76Zr}	24	76	D	✓	✓	✓
S_{86Zr}	14	86	E	✓	✓	✓
SF	×	×	×	✓	×	×
SS	87	13	A	×	✓	×
SSF	87	13	A	✓	✓	×

Based on the previous study [73], to prepare zirconia solution, 3.65 ml zirconium (IV) butoxide ($Zr(OC_4H_2)_4$, 80 wt.%, Sigma-Aldrich) and 0.63 gr citric acid ($C_6H_8O_7$, Merck) were dissolved in 125 ml absolute ethanol and stirred by a magnetic stirrer until a clear solution was obtained. Then, a combination of 2 gr PF127, 125 ml absolute ethanol, and 6.67 ml hydrochloric acid was gently added to the zirconia solution, stirred for 24 h with the speed of 1000 rpm at ambient temperature, and then aged for 48 h at a location with 40% humidity. Samples with different weight ratios of titania and zirconia solutions were prepared to investigate their effect on the sample integrity and microstructure. Table 1 shows the designation and specification of different samples.

PU sponge (60 PPI) with a mean pore size of 300-700 μm was used to make blocks with a dimension of 10 mm × 10 mm × 10 mm. The blocks were dipped in different solutions with various ZrO_2 to TiO_2 weight ratios for 1 h. The saturated PU blocks with the solution were squeezed by a hand roller. These blocks were then dried at room temperature for 72 h. The dried foams were sintered at 550°C for 2 h with the heating/cooling rate of 5°C min $^{-1}$. Figure 2 illustrates the preparation steps of different samples.

2.2. Sample Characterization. In order to assess the thermal decomposition temperature of PU foam and volatile materials and to optimize the calcination temperature of materials used to make the solutions, a simultaneous thermal analysis (STA) test was performed up to 550°C with the heating rate of 5°C/min, using the NETZSCH STA 449F3 machine.

To investigate the morphology and to measure the pore size of the scaffolds, scanning electron microscopy (SEM) was applied using SEM/EDS, Zeiss, Germany machine (FEI Quanta 200 SEM) with the working distance in the range of 9.5-13.8 μm and the voltage in the range of 15 to 25 kV. To evaluate the elemental compositions of samples, energy-dispersive spectroscopy (EDS) was utilized. Map scan analyses were performed to determine the elements formed in randomly selected locations of the scaffolds using the same machine. Small-angle X-ray scattering (SAXS) was performed using the Asenware AW-DX300 diffractometer to approve the formation of a mesoporous structure. SAXS traces were recorded with 2θ in the range of 0.5-10 degrees with a Cu Kα radiation source with $\lambda = 0.154184$ nm. Wide-angle X-ray diffraction (WAXRD) analysis with 2θ in the range of 10-90 degrees was used to study the crystalline phase of samples using the same machine. The nitrogen adsorption-desorption isotherms were used at 77 K using the BELSORP-mini II analyzer to determine the pore structure and to assess the specific surface area.

3. Results and Discussions

3.1. STA Evaluation. To assess the weight loss and to determine the temperature of reactions that occurred during the sintering procedure of TiO_2-ZrO_2 scaffolds, simultaneous thermal analysis (STA) was utilized. Different samples (Table 1, SS which contains only solution, SF which contains only PU foam, and SSF which contains a solution with PU foam together), 3 samples for each, were used to accurately determine the effect of each component on the STA traces. Figure 3 shows the results of the thermogravimetry-differential scanning calorimeter (TG-DSC) curves of different samples. The TG curve of the SF sample (contains only PU foam) showed that foam is burned out at a temperature of around 310 ± 2°C (Figure 3(a)) [74]. The results proved that at the sintering temperature, no sponge was left in the structure.

Figure 3(b) shows the STA analysis of the SS sample which only contains solution A (see Table 1). The results showed that there is an exothermic peak at 301.6°C. The TGA result also showed that this exothermic process accounted for a substantial amount of the total weight loss on the whole decomposition process from about 50°C to around 300°C. The exothermic peak and the associated weight loss were due to the decomposition of organic materials and their removal from the system, as proved by the EDS analysis of the sintered scaffolds, at 550°C in which no organic material was detected (Figure 4).

The exothermic peak and subsequent mass change at around 300°C were in good agreement with the reported results of previous studies. In other words, the range of around 171.40-301.37°C has been considered as the decomposition temperature of Pluronic F127. The decomposition temperature of zirconium butoxide, acetylacetone, titanium butoxide, and citric acid was reported to be around 176.85°C, 280°C, 122°C, and 19.85-399.85°C, respectively [72, 75–80].

Also, Figure 3(c) pertains to the SSF sample, the one with both foam and solution. It can be seen that foam was removed from the system at 283.6 ± 2°C. The exothermic peak occurred at 434.9 ± 1°C could be ascribed to the oxidation of titanium and zirconium. Based on the results of Figure 3, the calcination temperature was adjusted to 550°C to ensure that at the end of the heat treatment cycle, no foam

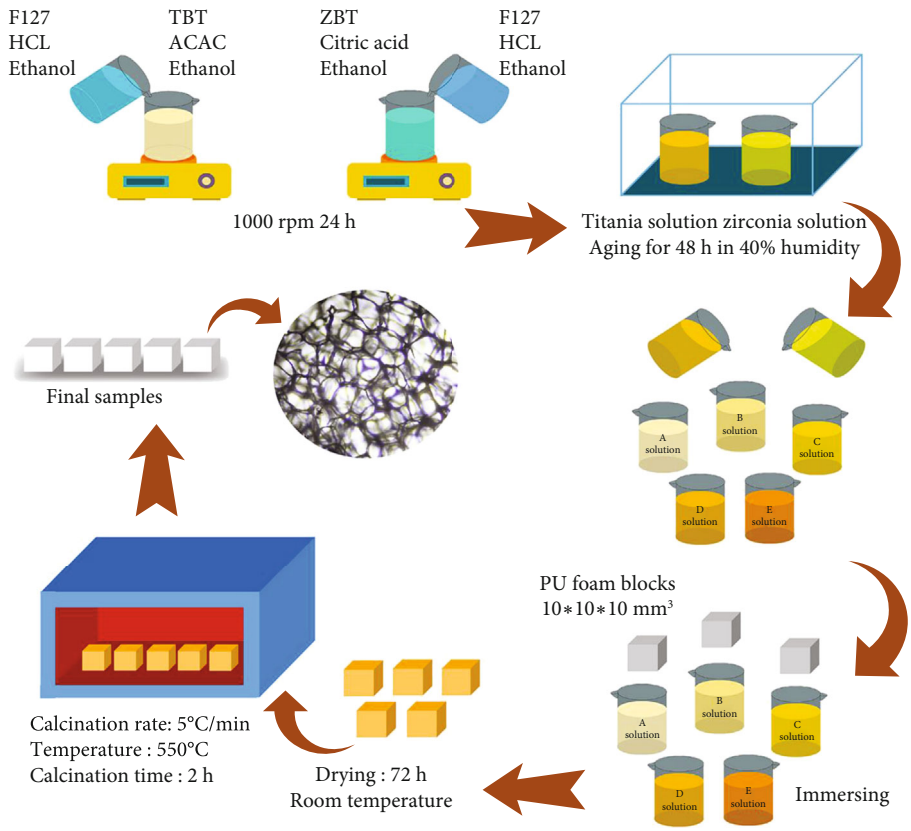

Figure 2: Schematic representation of the synthesis procedure of meso/macroporous TiO_2-ZrO_2 scaffolds.

and organic additives were left in the scaffolds and only titanium and zirconium oxides were present in the structure.

3.2. SEM/EDS Evaluation. The morphology and pore size of the scaffolds are extremely important to achieve desirable mechanical properties and to have effective cell adhesion, cell proliferation, and strong cell growth into the scaffolds. The optimized sample in this study was known as the one with structural integrity without any cracks. To investigate the morphology of pores that have been formed through the foamy method after heat treatment and their size, samples were studied with SEM. Figure 5 shows the structure, pore morphology, pore size, pore distribution, mesopores, and finally pore wall of a random macropore of S_{13Zr} sample which was annealed at 550°C for 2 h. Figures 5(a) and 5(b) show the macropore structure, and Figures 5(c) and 5(d) show the mesopore structures in the scaffolds.

On the other hand, Figure 6 shows the structure of other samples with different amounts of zirconia that were annealed in the same condition. As can be seen in Figure 6, all samples have some structural defects such as cracks on the wall of pores (shown by arrows). The high amount of zirconia can be the reason for the existence of cracks in the scaffolds which makes them completely useless for bone tissue engineering applications [61]. However, as can be seen in Figure 5, S_{13Zr} sample (containing 13 wt.% zirconia and 87 wt.% titania) exhibits an integrated structure with no crack, appropriate pore size for cell accommodation, cell growth, and cell proliferation. Therefore, S_{13Zr} sample was considered as the optimized sample for further studies.

Figure 7 shows the histogram of the macropore size in the S_{13Zr} sample. As it is obvious, the formation of appropriate macroporosity with a desirable size (more frequency in pore sizes measured greater than 150 μm that is beneficial for cell accommodation, penetration, and differentiation) in the produced scaffold can provide a suitable environment for the vascularization which plays a vital role in the success of the scaffold. EDS was utilized to reveal the average local chemical composition in the produced scaffold. Figure 4 shows the EDS results of the S_{13Zr} sample. A homogeneous distribution of Ti and Zr elements was observed in the EDS results of the optimized scaffold.

Figure 8 shows the results of the EDS elemental mapping of the S_{13Zr} sample. The results showed a homogeneous distribution of Ti and Zr in this sample which demonstrate the effectiveness of the fabrication technique to form a uniform structure.

3.3. XRD Evaluation. The phase transformation of the S_{13Zr} sample was investigated by XRD. Figure 9(a) illustrates the wide-angle X-ray scattering (WAXRD) pattern. The presence of metal oxide formed at the low temperature was successfully proved by the XRD patterns. As can be seen in Figure 9(a), the sample has not been completely crystallized due to the low temperature used for heat treatment. The low annealing temperature was used to protect and retain the mesopores of the sample because the mesopores will collapse

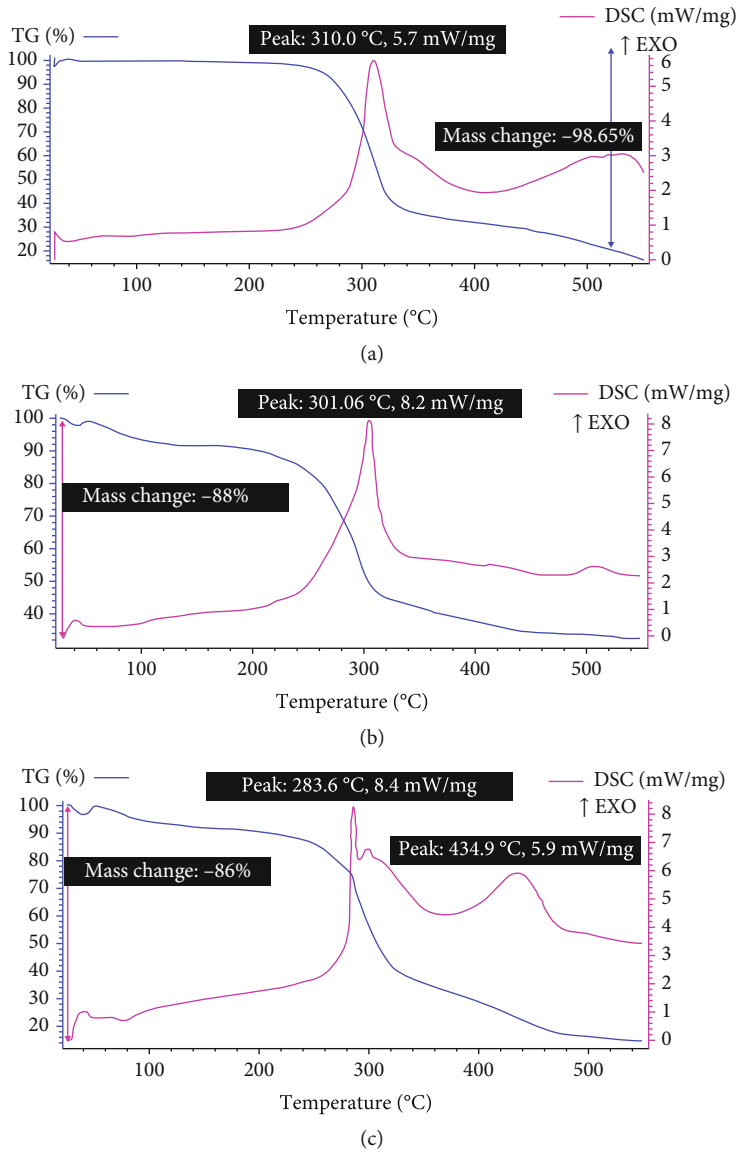

Figure 3: (a) Simultaneous thermal analysis of PU foam; (b) simultaneous thermal analysis of solution A (see Table 1); (c) simultaneous thermal analysis of SFF sample.

during a high temperature of sintering [81]. On the other hand, the mesoporous structure transforms the long-range order of crystals into the short-range order. So the XRD pattern of mesoporous structures is similar to semicrystalline structures [81]. An intensive peak can be seen in Figure 9(a) in 2θ equals to 25 degrees that shows the formation of the anatase phase (XRD JCPDS data file No. 01-071-1169) in the structure.

Titania and zirconia can form different crystal polymorphs at different temperatures [82, 83]. According to their phase diagram and the calcination temperature, the anatase phase for titania and monoclinic phase for zirconia should be stable at room temperature [84].

Based on the literature, the monoclinic phase of zirconia is thermodynamically its most stable phase; however, the less stable phases of zirconia (cubic or tetragonal) could form at higher temperatures. In other words, according to the zirconia phase diagram, the monoclinic phase of zirconia is stable from ambient temperature to 1170°C. The tetragonal phase is stable from 1170°C to 2370°C, and from 2370°C to the melting point cubic phase of zirconia will be stable [83].

On the other hand, the most stable phase of titania is rutile; however, according to previous studies, the formation of short-range order TiO_6 in anatase is easier than the formation of long-range order TiO_6 in rutile [82]. Also, thermodynamically, the level of surface free energy of anatase is lower than that of the rutile phase which causes that TiO_2-based nanocomposites and nanofilms contain anatase phase at room temperature [82].

Some elements such as Ca, scandium, strontium, yttrium, niobium, barium, lanthanum, aurum (gold), boron, aluminum, silicon, phosphorus, sulfur, chlorine, cerium, neodymium, samarium, europium, gadolinium, terbium, dysprosium,

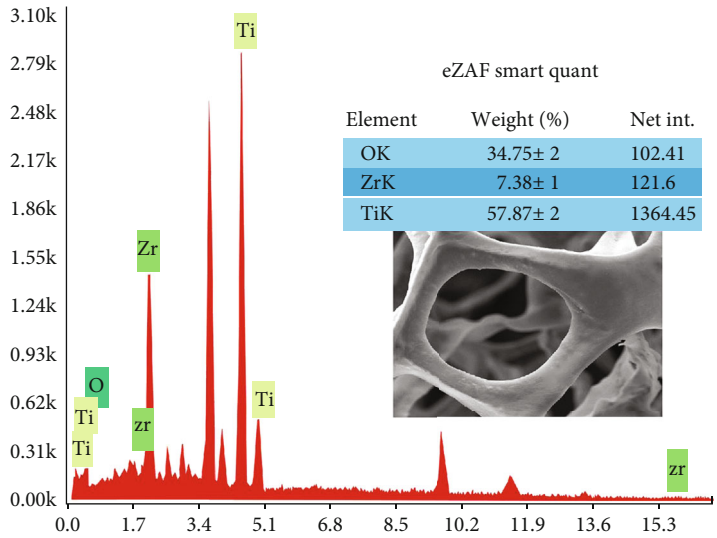

Figure 4: EDAX analysis of the S_{13Zr} sample.

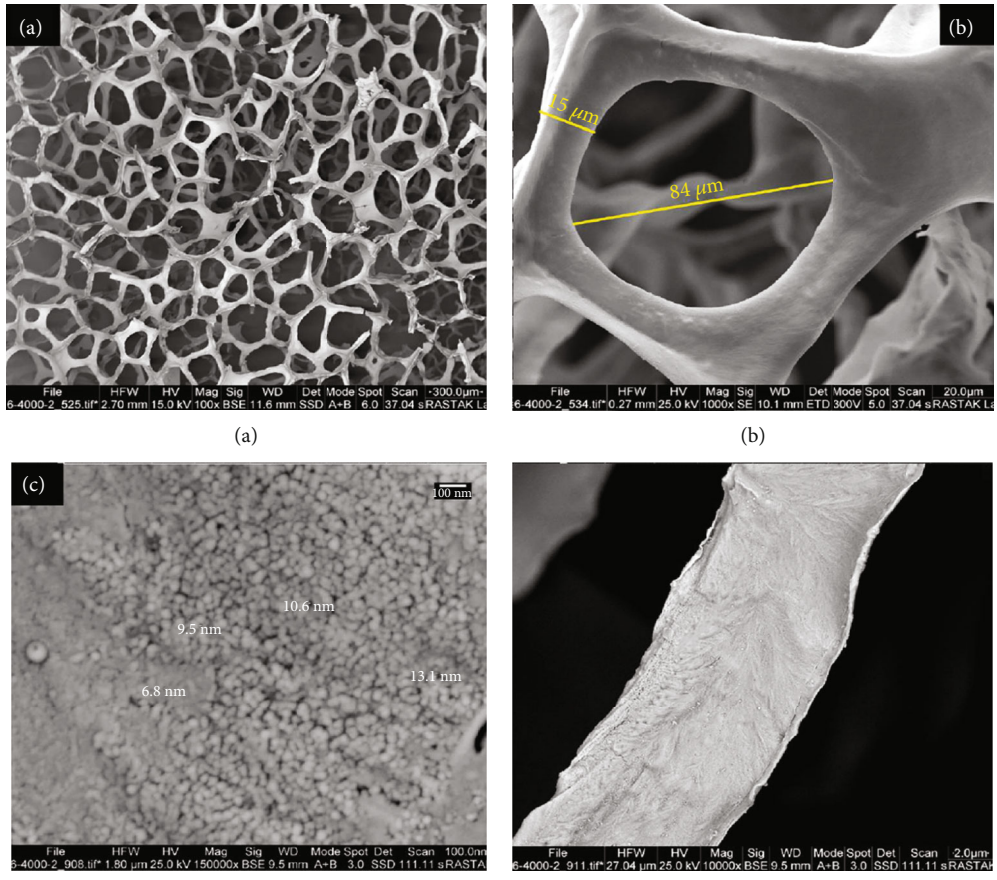

(a) (b) (c) (d)

Figure 5: Scanning electron microscopy (SEM) images of sample S_{13Zr} as the optimized sample (S_{13Zr}) sintered at 550°C for 2 h: (a) the general shape of the scaffold which shows the favorable structural integrity, (b) acceptable pore morphology and pore size (no crack can be observed), (c) desirable size of mesopores which are the best space to insert nutrients to be used by cells in order to proliferate and grow into the scaffold, and (d) strong pore wall which exhibits nice interconnectivity and strong structure for each macropore to mimic the natural bone tissue structure.

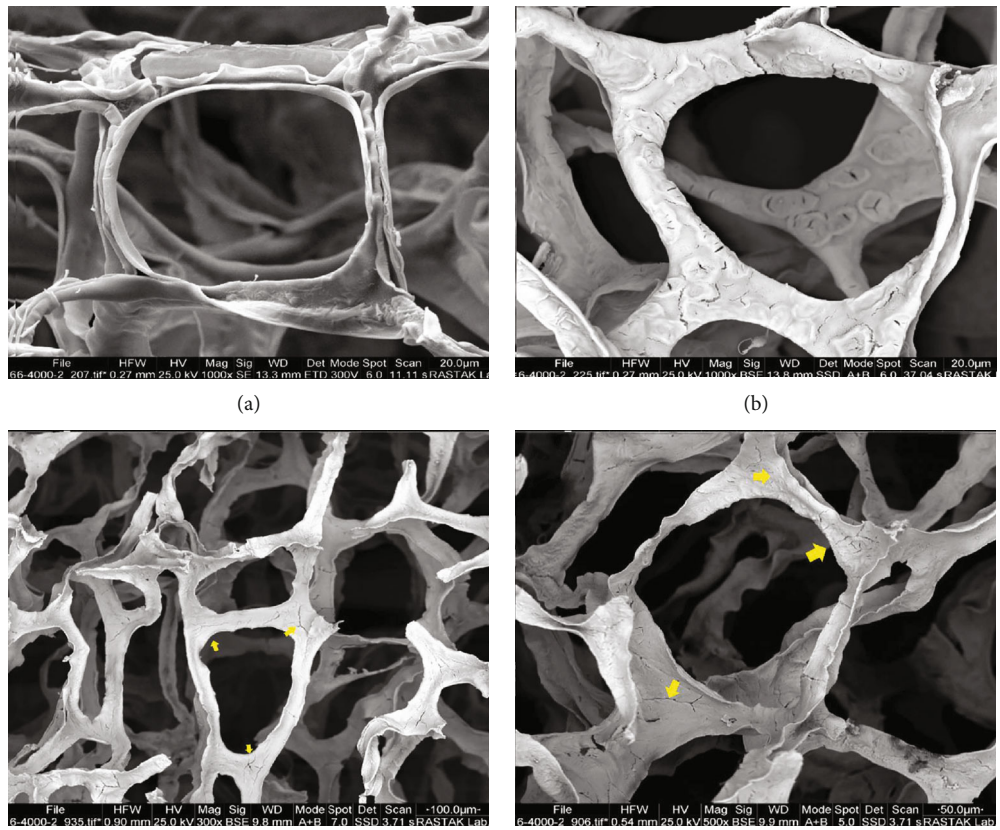

FIGURE 6: Scanning electron microscopy (SEM) images of (a) sample S_{26Zr}, (b) sample S_{50Zr}, (c) sample S_{76Zr}, and (d) sample S_{86Zr} which are completely inappropriate for cells to attach and grow in. It seems that the different amount of zirconia and titania has made heterogeneity in their structure which results in forming cracks and weak pores and pore walls and also the high amount of zirconia in the samples has a detrimental role in structural integrity.

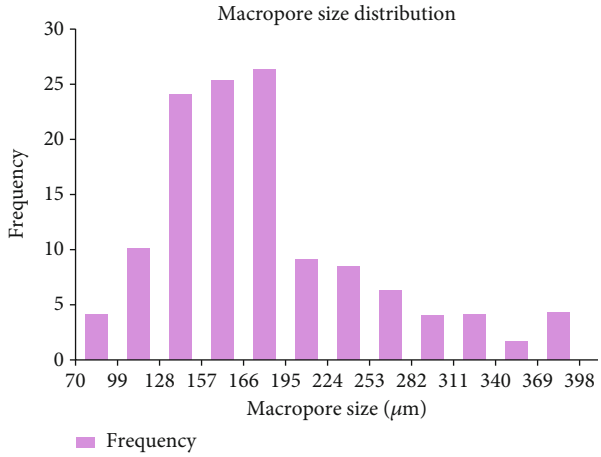

FIGURE 7: The histogram of the macropore size distribution in the S_{13Zr} sample.

holmium, erbium, thulium, ytterbium, and specifically zirconia have an inhibitor role against phase transformation from anatase to rutile in titania [4, 82, 85]. In this study, Zr has been used as the second phase of the nanocomposite. In fact, the addition of zirconia to titania stabilizes the anatase phase of titania and inhibits its grain growth [86].

Figure 9(b) shows the small-angle X-ray spectroscopy (SAXS) pattern of sample S_{13Zr} which was sintered at 550° for 2 h. In the SAXS analysis, the intensity and sharpness of the peak is a sign of the formation of a well-ordered mesoporous structure [87, 88]. SAXS was performed in the 2θ range of 0.5-10 degrees. As can be seen in Figure 9(b), a sharp peak in 2θ equals to 0.7 degrees can be observed which indicates the formation of well-ordered mesoporous structures in this sample. The results obtained from the SAXS analysis were in good agreement with those obtained from the SEM observation (Figure 5(c)).

In general, TiO_2 formation occurs in three different steps. As mentioned, the sol-gel method through the alkoxide route was used to prepare TiO_2 and ZrO_2 solutions. At the first step, the aqueous environment induces alkoxide hydrolysis and produces titanium hydroxide and zirconium hydroxide and alcohol (alkoxide group hydroxide). The second step can occur through the interaction between either two hydroxide metals or a hydroxide metal and an alkoxide metal that finally produce A-O-A, in which A refers to the metal (Zr or Ti) and O refers to the oxygen, and water or alcohol in an aqueous and alcoholic environment [89–91]. TiO_2 and ZrO_2 particles act as the nuclei to expand metal oxides formed during the synthesis procedure. The steps of the formation of TiO_2 can be expressed as follows [90]:

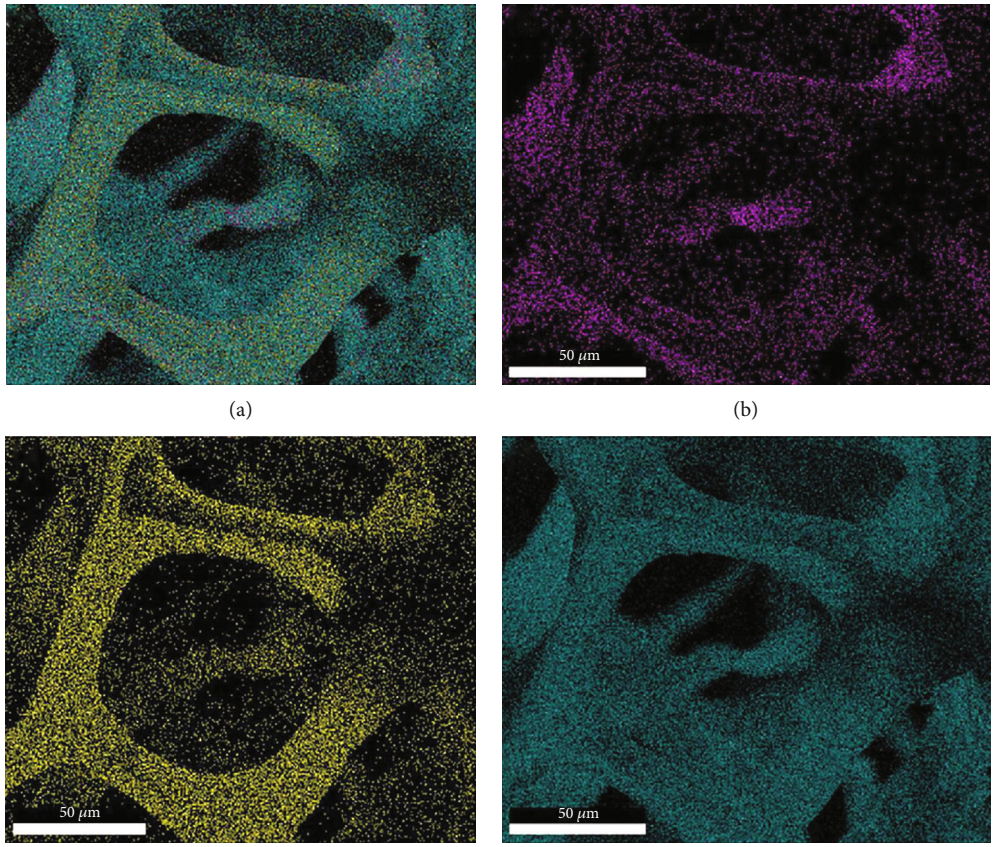

Figure 8: EDX elemental mapping of S_{13Zr} sample: (a) oxygen (5 wt.%), zirconium (12 wt.%), and titanium (83 wt.%); (b) oxygen; (c) zirconium; (d) titanium.

(1) Hydrolysis of titanium alkoxide:

$$C_{16}H_{36}O_4Ti + 4H_2O \longrightarrow Ti(OH)_4 + 4C_4H_9OH \quad (1)$$

(2) Condensation of hydrolyzed species:

$$Ti(OH)_4 \longrightarrow TiO_2 + 2H_2O \quad (2)$$

Equation (2) can also be expressed as follows:

$$\begin{aligned}&\text{Water condensation}: Ti(OH)_4 + Ti(OH)_4 \longrightarrow Ti—O—Ti + HOH\\ &\text{Alcohol condensation}: Ti(OH)_4 + Ti(OC_4H_9)_4 \longrightarrow Ti—O—Ti\\ &\quad + C_4H_9OHTiO_2 \text{ sol particles}\end{aligned} \quad (3)$$

(3) Growth of TiO_2 sol particles

On the other hand, almost the same procedures happen during the formation of ZrO_2 [91]:

(1) Hydrolysis of zirconium alkoxide:

$$C_{16}H_8O_4Zr + H_2O \longrightarrow Zr(OH)_4 + C_{16}H_8O_4(OH) \quad (4)$$

(2) Condensation of hydrolyzed species:

$$Zr(OH)_4 + ZrO_4H_{36}C_{16} \longrightarrow Zr - O - Zr + C_{16}H_{36}O_4(OH) \quad (5)$$

In more details:

$$\begin{aligned}&\text{Water condensation}: Zr(OH)_4 + Zr(OH)_4 \longrightarrow Zr—O—Zr + HOH\\ &\text{Alcohol condensation}: Zr(OH)_4 + Zr(OR)_4 \longrightarrow Zr—O—Zr\\ &\quad + C_4H_9OHZrO_2 \text{ sol particles}\end{aligned} \quad (6)$$

(3) Growth of ZrO_2 sol particles

Figure 10 shows the schematic representation of the aforementioned steps clearly in detail.

The nuclei growth phenomenon stems from the incredible high surface area of particles and consequently their high

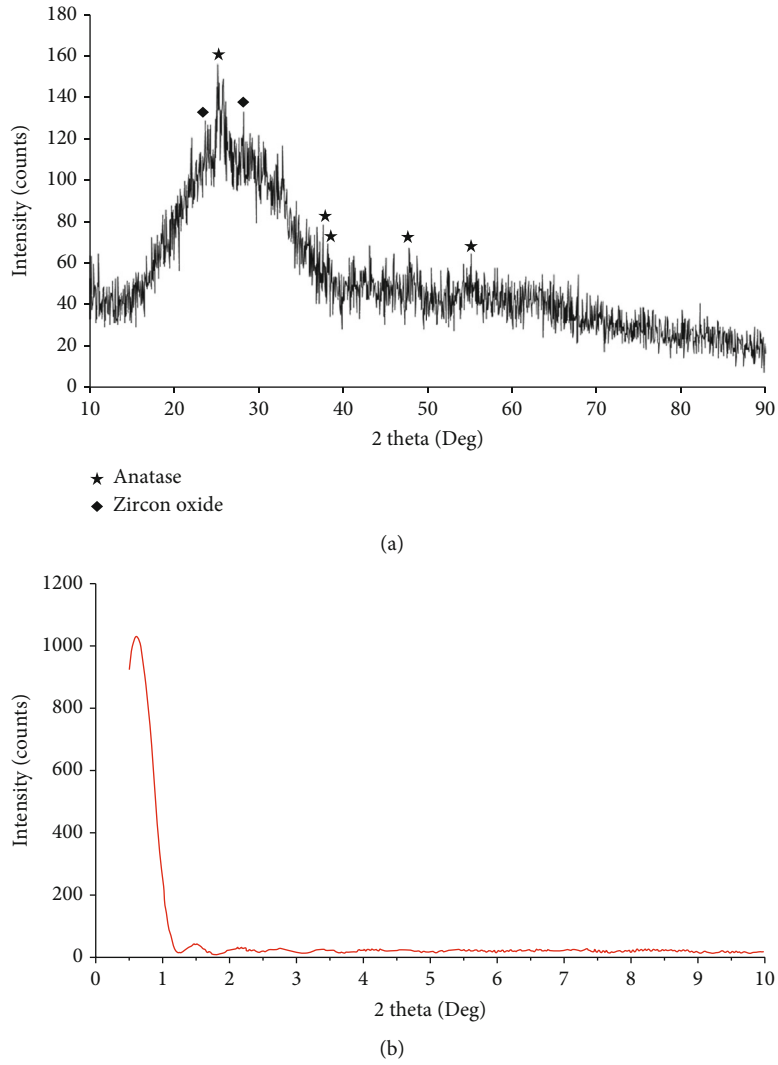

FIGURE 9: (a) Wide-angle XRD of the optimized sample contains 13 wt.% ZrO_2 and 87 wt.% TiO_2 heated at 550°C for 2 h with the heating/cooling rate of 5°C min^{-1}. (b) Small-angle XRD of optimized meso/macroporous titania-zirconia sample heated at 550°C for 2 h.

amount of energy which makes them thermodynamically unstable. For this purpose, metal oxide particles (as the nuclei) start to grow through Ostwald ripening or oriented attachment mechanism or even both, to decrease their energy level. According to Ostwald ripening phenomenon, small particles dissolve in the solution because of their high energy level and bigger particles get bigger and bigger in regular spherical shapes by attracting small particles. Based on the oriented attachment mechanism, small particles get together and aggregate at the first step; then, they will be considered as a specific place for other small particles to attach and consequently form crystals [92]. Linear F127 polymer that was used as the template for mesopores has hydrophilic and hydrophobic parts. After dissolving in ethanol, F127 forms special structures that usually transforms into regular spherical micelles in solution. Finally, drying and calcination cause the formation of mesostructure [93]. Figure 11 shows the mechanism of mesopore formation.

3.4. BET Evaluation. Figure 12 demonstrates the nitrogen adsorption-desorption isotherms of the S_{13Zr} sample after sintering at 550°C for 2 h. The specific surface area of the S_{13Zr} sample measured by the Brunauer-Emmett-Teller (BET) theory was 13.627 m^2g^{-1}; the total porosity volume obtained from the adsorption curve of the isotherm diagram and mean pore diameter were 0.03788 cm^3g^{-1} and 11.119 nm, respectively.

4. Conclusions

In this study, hierarchical meso/macroporous hierarchical titania-zirconia nanocomposite was fabricated for tissue engineering applications. Different samples with different weight percentages of titania and zirconia were prepared by the help of the EISA technique coupled with the foamy method. The foamy method was applied to provide the macropore template, and the EISA method was utilized to

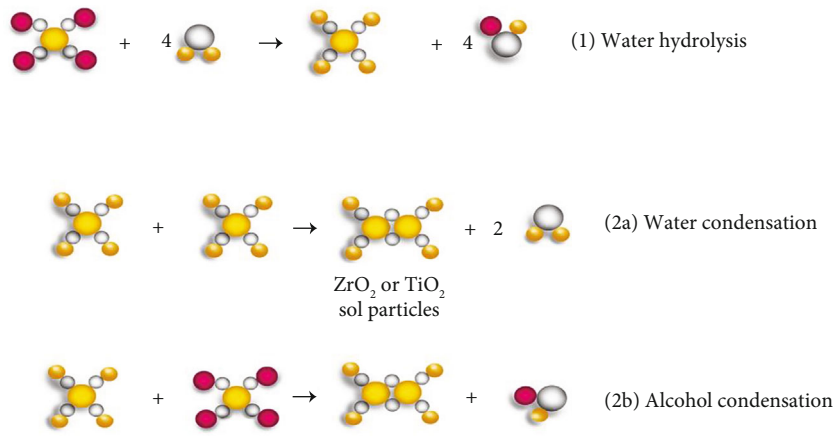

Figure 10: Schematic representation of chemical interactions involved in the sol-gel process.

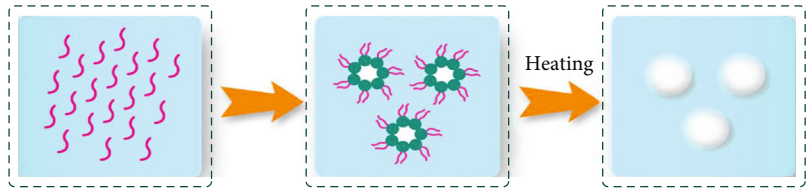

Figure 11: Schematic representation of mesopore formation mechanism and the behavior of F127 linear polymer in the solution.

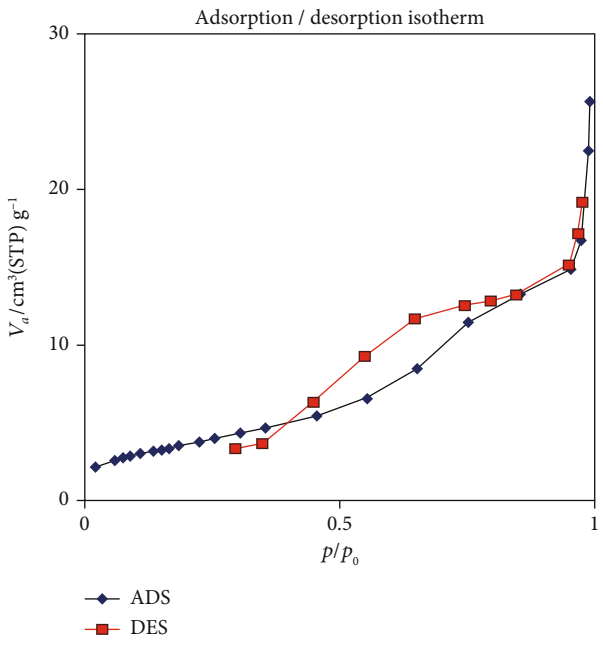

Figure 12: BET analysis of the S_{13Zr} scaffold as the optimized sample.

provide a mesopore structure. The results showed that scaffolds with a lower amount of zirconia had less structural defects. This scaffold had pore size, pore wall size, and mesopores in the range of $185 \pm 66\,\mu$m, $15 \pm 4\,\mu$m, and 7-13 nm, respectively. The specific surface area obtained from the BET theory, total volume, and mean diameter of pores of this sample was 13.627 m^2g^{-1}, 0.03788 cm^3g^{-1}, and 11 nm, respectively.

Data Availability

The raw/processed data required to reproduce these findings cannot be shared at this time as the data also forms part of an ongoing study. If you need to have access to some of the raw data, please contact the corresponding author.

Additional Points

Highlights. (1) ZrO_2/TiO_2 nanocomposite scaffolds were synthesized using the EISA and foamy method. (2) The formation mechanism of the scaffolds was scrutinized. (3) The influence of the ZrO_2 on the integrity of the scaffolds was evaluated. (4) Nanocomposite scaffolds consisting of 13 wt.% ZrO_2 showed an integrated structure

Conflicts of Interest

The authors declare that there is no conflict of interest regarding the publication of this article.

References

[1] A. R. Amini, C. T. Laurencin, and S. P. Nukavarapu, "Bone tissue engineering: recent advances and challenges," *Critical Reviews in Biomedical Engineering*, vol. 40, no. 5, pp. 363–408, 2012.

[2] S. Bose, M. Roy, and A. Bandyopadhyay, "Recent advances in bone tissue engineering scaffolds," *Trends in Biotechnology*, vol. 30, no. 10, pp. 546–554, 2012.

[3] K. J. L. Burg, S. Porter, and J. F. Kellam, "Biomaterial developments for bone tissue engineering," *Biomaterials*, vol. 21, no. 23, pp. 2347–2359, 2000.

[4] C. Chen, E. Kelder, and J. Schoonman, "Electrostatic sol-spray deposition (ESSD) and characterisation of nanostructured TiO_2 thin films," *Thin Solid Films*, vol. 342, no. 1-2, pp. 35–41, 1999.

[5] C. J. Damien and J. R. Parsons, "Bone graft and bone graft substitutes: a review of current technology and applications," *Journal of Applied Biomaterials*, vol. 2, no. 3, pp. 187–208, 1991.

[6] P. V. Giannoudis, H. Dinopoulos, and E. Tsiridis, "Bone substitutes: an update," *Injury*, vol. 36, no. 3, pp. S20–S27, 2005.

[7] L. G. Griffith and G. Naughton, "Tissue engineering–current challenges and expanding opportunities," *Science*, vol. 295, no. 5557, pp. 1009–1014, 2002.

[8] L. L. Hench, "Bioceramics: from concept to clinic," *Journal of the American Ceramic Society*, vol. 74, no. 7, pp. 1487–1510, 1991.

[9] J. Henkel, M. A. Woodruff, D. R. Epari et al., "Bone regeneration based on tissue engineering conceptions — a 21st century perspective," *Bone Research*, vol. 1, no. 3, pp. 216–248, 2013.

[10] J. R. Jones and L. L. Hench, "Regeneration of trabecular bone using porous ceramics," *Current Opinion in Solid State and Materials Science*, vol. 7, no. 4-5, pp. 301–307, 2003.

[11] D. C. Lobb, B. R. DeGeorge Jr., and A. B. Chhabra, "Bone Graft Substitutes: current concepts and future expectations," *The Journal of Hand Surgery*, vol. 44, no. 6, pp. 497–505.e2, 2019.

[12] P. X. Ma, "Scaffolds for tissue fabrication," *Materials Today*, vol. 7, no. 5, pp. 30–40, 2004.

[13] A. G. Mikos, S. W. Herring, P. Ochareon et al., "Engineering complex tissues," *Tissue Engineering*, vol. 12, no. 12, pp. 3307–3339, 2006.

[14] R. G. Ribas, V. M. Schatkoski, T. L. d. A. Montanheiro et al., "Current advances in bone tissue engineering concerning ceramic and bioglass scaffolds: A review," *Ceramics International*, vol. 45, no. 17, pp. 21051–21061, 2019.

[15] F. R. A. J. Rose and R. O. C. Oreffo, "Bone tissue engineering: hope vs hype," *Biochemical and Biophysical Research Communications*, vol. 292, no. 1, pp. 1–7, 2002.

[16] A. J. Salinas, P. Esbrit, and M. Vallet-Regí, "A tissue engineering approach based on the use of bioceramics for bone repair," *Biomaterials Science*, vol. 1, no. 1, pp. 40–51, 2013.

[17] B. D. Smith and D. A. Grande, "The current state of scaffolds for musculoskeletal regenerative applications," *Nature Reviews Rheumatology*, vol. 11, no. 4, pp. 213–222, 2015.

[18] M. M. Stevens, "Biomaterials for bone tissue engineering," *Materials Today*, vol. 11, no. 5, pp. 18–25, 2008.

[19] J. Vacanti, "Tissue engineering and regenerative medicine: from first principles to state of the art," *Journal of Pediatric Surgery*, vol. 45, no. 2, pp. 291–294, 2010.

[20] W. Wang and K. W. K. Yeung, "Bone grafts and biomaterials substitutes for bone defect repair: a review," *Bioactive Materials*, vol. 2, no. 4, pp. 224–247, 2017.

[21] S. Yang, K.-F. Leong, Z. Du, and C.-K. Chua, "The design of scaffolds for use in tissue engineering. Part I. Traditional factors," *Tissue Engineering*, vol. 7, no. 6, pp. 679–689, 2001.

[22] X. Yu, X. Tang, S. V. Gohil, and C. T. Laurencin, "Biomaterials for bone regenerative engineering," *Advanced Healthcare Materials*, vol. 4, no. 9, pp. 1268–1285, 2015.

[23] K. Zhang, S. Wang, C. Zhou et al., "Advanced smart biomaterials and constructs for hard tissue engineering and regeneration," *Bone Research*, vol. 6, no. 1, pp. 1–15, 2018.

[24] M. J. Olszta, X. Cheng, S. S. Jee et al., "Bone structure and formation: A new perspective," *Materials Science and Engineering: R: Reports*, vol. 58, no. 3-5, pp. 77–116, 2007.

[25] S. H. Ralston, "Bone structure and metabolism," *Medicine*, vol. 41, no. 10, pp. 581–585, 2013.

[26] J. Buckwalter and R. Cooper, "Bone structure and function," *Instructional Course Lectures*, vol. 36, pp. 27–48, 1987.

[27] J. R. Jones, P. D. Lee, and L. L. Hench, "Hierarchical porous materials for tissue engineering," *Philosophical Transactions of the Royal Society A: Mathematical, Physical and Engineering Sciences*, vol. 364, no. 1838, pp. 263–281, 2006.

[28] J.-Y. Rho, L. Kuhn-Spearing, and P. Zioupos, "Mechanical properties and the hierarchical structure of bone," *Medical Engineering & Physics*, vol. 20, no. 2, pp. 92–102, 1998.

[29] S. Weiner and W. Traub, "Bone structure: from ångstroms to microns," *The FASEB Journal*, vol. 6, no. 3, pp. 879–885, 1992.

[30] J. X. Lu, B. Flautre, K. Anselme et al., "Role of interconnections in porous bioceramics on bone recolonization in vitro and in vivo," *Journal of Materials Science Materials in Medicine*, vol. 10, no. 2, pp. 111–120, 1999.

[31] M. Mastrogiacomo, S. Scaglione, R. Martinetti et al., "Role of scaffold internal structure on in vivo bone formation in macroporous calcium phosphate bioceramics," *Biomaterials*, vol. 27, no. 17, pp. 3230–3237, 2006.

[32] B. Feng, Z. Jinkang, W. Zhen et al., "The effect of pore size on tissue ingrowth and neovascularization in porous bioceramics of controlled architecturein vivo," *Biomedical Materials*, vol. 6, no. 1, article 015007, 2011.

[33] V. Karageorgiou and D. Kaplan, "Porosity of 3D biomaterial scaffolds and osteogenesis," *Biomaterials*, vol. 26, no. 27, pp. 5474–5491, 2005.

[34] C. M. Murphy, M. G. Haugh, and F. J. O'brien, "The effect of mean pore size on cell attachment, proliferation and migration in collagen–glycosaminoglycan scaffolds for bone tissue engineering," *Biomaterials*, vol. 31, no. 3, pp. 461–466, 2010.

[35] J. Zeltinger, J. K. Sherwood, D. A. Graham, R. Müeller, and L. G. Griffith, "Effect of pore size and void fraction on cellular adhesion, proliferation, and matrix deposition," *Tissue Engineering*, vol. 7, no. 5, pp. 557–572, 2001.

[36] W. Zhen, C. Jiang, B. Feng, S. Xiaojiang, L. Jianxi, and L. Li, "Role of the porous structure of the bioceramic scaffolds in bone tissue engineering," *Nature Precedings*, 2010.

[37] D. Lozano, M. Manzano, J. C. Doadrio et al., "Osteostatin-loaded bioceramics stimulate osteoblastic growth and differentiation," *Acta Biomaterialia*, vol. 6, no. 3, pp. 797–803, 2010.

[38] J. Rouwkema and A. Khademhosseini, "Vascularization and angiogenesis in tissue engineering: beyond creating static networks," *Trends in Biotechnology*, vol. 34, no. 9, pp. 733–745, 2016.

[39] J. Rouwkema, N. Rivron, and C. A. van Blitterswijk, "Vascularization in tissue engineering," *Trends in Biotechnology*, vol. 26, no. 8, pp. 434–441, 2008.

[40] W. Tang, D. Lin, Y. Yu et al., "Bioinspired trimodal macro/micro/nano-porous scaffolds loading rhBMP-2 for complete regeneration of critical size bone defect," *Acta Biomaterialia*, vol. 32, pp. 309–323, 2016.

[41] C. Wu and J. Chang, "Mesoporous bioactive glasses: structure characteristics, drug/growth factor delivery and bone regeneration application," *Review Interface Focus*, vol. 2, no. 3, pp. 292–306, 2012.

[42] S. Yang, K. Leong, Z. du, and C. K. Chua, "The design of scaffolds for use in tissue engineering. Part II. Rapid prototyping techniques," *Tissue Engineering*, vol. 8, no. 1, pp. 1–11, 2002.

[43] O. Sel, D. Kuang, M. Thommes, and B. Smarsly, "Principles of hierarchical meso- and macropore architectures by liquid crystalline and polymer colloid templating," *Langmuir*, vol. 22, no. 5, pp. 2311–2322, 2006.

[44] B. Smarsly and M. Antonietti, "Block copolymer assemblies as templates for the generation of mesoporous inorganic materials and crystalline films," *European Journal of Inorganic Chemistry*, vol. 2006, no. 6, pp. 1111–1119, 2006.

[45] S. Deville, "Freeze-casting of porous ceramics: a review of current achievements and issues," *Advanced Engineering Materials*, vol. 10, no. 3, pp. 155–169, 2008.

[46] M. C. Gutiérrez, M. L. Ferrer, and F. del Monte, "Ice-templated materials: sophisticated structures exhibiting enhanced functionalities obtained after unidirectional freezing and ice-segregation-induced self-assembly†," *Chemistry of Materials*, vol. 20, no. 3, pp. 634–648, 2008.

[47] L. Qian and H. Zhang, "Controlled freezing and freeze drying: a versatile route for porous and micro-/nano-structured materials," *Journal of Chemical Technology and Biotechnology*, vol. 86, no. 2, pp. 172–184, 2011.

[48] A. Feinle, M. S. Elsaesser, and N. Hüsing, "Sol–gel synthesis of monolithic materials with hierarchical porosity," *Chemical Society Reviews*, vol. 45, no. 12, pp. 3377–3399, 2016.

[49] A. Monnier, F. Schüth, Q. Huo et al., "Cooperative formation of inorganic-organic interfaces in the synthesis of silicate mesostructures," *Science*, vol. 261, no. 5126, pp. 1299–1303, 1993.

[50] L. W. Hench and J. K. West, "The sol-gel process," *Chemical Reviews*, vol. 90, no. 1, pp. 33–72, 1990.

[51] Y. Lu, H. Fan, A. Stump, T. L. Ward, T. Rieker, and C. J. Brinker, "Aerosol-assisted self-assembly of mesostructured spherical nanoparticles," *Nature*, vol. 398, no. 6724, pp. 223–226, 1999.

[52] H. Yang, N. Coombs, I. Sokolov, and G. A. Ozin, "Free-standing and oriented mesoporous silica films grown at the air–water interface," *Nature*, vol. 381, no. 6583, pp. 589–592, 1996.

[53] C. J. Brinker, "Evaporation-induced self-assembly: functional nanostructures made easy," *MRS Bulletin*, vol. 29, no. 9, pp. 631–640, 2004.

[54] G. J. Soler-Illia, P. C. Angelomé, M. C. Fuertes, D. Grosso, and C. Boissiere, "Critical aspects in the production of periodically ordered mesoporous titania thin films," *Nanoscale*, vol. 4, no. 8, pp. 2549–2566, 2012.

[55] G. Soler-Illia, C. Sanchez, B. Lebeau, and J. Patarin, "Chemical strategies to design textured materials: from microporous and mesoporous oxides to nanonetworks and hierarchical structures," *Chemical Reviews*, vol. 102, no. 11, pp. 4093–4138, 2002.

[56] P. Yang, D. Zhao, D. I. Margolese, B. F. Chmelka, and G. D. Stucky, "Generalized syntheses of large-pore mesoporous metal oxides with semicrystalline frameworks," *Nature*, vol. 396, no. 6707, pp. 152–155, 1998.

[57] H. Luo, C. Wang, and Y. Yan, "Synthesis of mesostructured titania with controlled crystalline framework," *Chemistry of Materials*, vol. 15, no. 20, pp. 3841–3846, 2003.

[58] X. Fu, L. A. Clark, Q. Yang, and M. A. Anderson, "Enhanced photocatalytic performance of titania-based binary metal oxides: TiO2/SiO2and TiO2/ZrO2," *Science and Technology*, vol. 30, no. 2, pp. 647–653, 1996.

[59] J. C. Yu, J. Lin, and R. W. M. Kwok, "Ti1-xZrxO2solid solutions for the photocatalytic degradation of acetone in air," *The Journal of Physical Chemistry. B*, vol. 102, no. 26, pp. 5094–5098, 1998.

[60] J. Marchi, E. M. Amorim, D. R. R. Lazar, V. Ussui, A. H. A. Bressiani, and P. F. Cesar, "Physico-chemical characterization of zirconia–titania composites coated with an apatite layer for dental implants," *Dental Materials*, vol. 29, no. 9, pp. 954–962, 2013.

[61] H. Tiainen, G. Eder, O. Nilsen, and H. J. Haugen, "Effect of ZrO_2 addition on the mechanical properties of porous TiO_2 bone scaffolds," *Materials Science and Engineering: C*, vol. 32, no. 6, pp. 1386–1393, 2012.

[62] V. Damodaran, D. Bhatnagar, V. Leszczak, and K. C. Popat, "Titania nanostructures: a biomedical perspective," *RSC Advances*, vol. 5, no. 47, pp. 37149–37171, 2015.

[63] M. Hamzeh and G. I. Sunahara, "*In vitro* cytotoxicity and genotoxicity studies of titanium dioxide (TiO_2) nanoparticles in Chinese hamster lung fibroblast cells," *Toxicology in Vitro*, vol. 27, no. 2, pp. 864–873, 2013.

[64] T. Kokubo, T. Matsushita, and H. Takadama, "Titania-based bioactive materials," *Journal of the European Ceramic Society*, vol. 27, no. 2-3, pp. 1553–1558, 2007.

[65] R. L. Hentrich, G. A. Graves, H. G. Stein, and P. K. Bajpai, "An evaluation of inert and resorbale ceramics for future clinical orthopedic applications," *Journal of Biomedical Materials Research*, vol. 5, no. 1, pp. 25–51, 1971.

[66] P. F. Manicone, P. Rossi Iommetti, and L. Raffaelli, "An overview of zirconia ceramics: basic properties and clinical applications," *Journal of Dentistry*, vol. 35, no. 11, pp. 819–826, 2007.

[67] C. Piconi and G. Maccauro, "Zirconia as a ceramic biomaterial," *Biomaterials*, vol. 20, no. 1, pp. 1–25, 1999.

[68] T. Thamaraiselvi and S. Rajeswari, "Trends Biomater," *Artificial Organs*, vol. 18, 2003.

[69] K. Houjou, K. Ando, and K. Takahashi, "Crack -Healing Behaviour of Zirconia/SiC Composite Ceramics," *Journal of the Society of Materials Science, Japan*, vol. 58, no. 6, pp. 510–515, 2009.

[70] K. Houjou, S. Sudo, and K. Takahashi, "Crack-Healing Behaviour of Zirconia /SiC Composite Ceramics and Strength Properties of Crack-Healing Specimens," *Journal of the Society of Materials Science, Japan*, vol. 60, no. 8, pp. 742–747, 2011.

[71] F. Samanipour, M. R. Bayati, F. Golestani-Fard, H. R. Zargar, T. Troczynski, and A. R. Mirhabibi, "An innovative technique to simply fabricate ZrO_2–HA–TiO_2 nanostructured layers," *Colloids and Surfaces B: Biointerfaces*, vol. 86, no. 1, pp. 14–20, 2011.

[72] S. M. Mirhadi, N. Hassanzadeh Nemati, F. Tavangarian, and M. Daliri Joupari, "Fabrication of hierarchical meso/macroporous TiO2 scaffolds by evaporation-induced self-assembly technique for bone tissue engineering applications," *Materials Characterization*, vol. 144, pp. 35–41, 2018.

[73] S. K. Das, M. K. Bhunia, A. K. Sinha, and A. Bhaumik, "Self-assembled mesoporous zirconia and sulfated zirconia nanoparticles synthesized by triblock copolymer as template," *Journal of Physical Chemistry C*, vol. 113, no. 20, pp. 8918–8923, 2009.

[74] J. Chambers and C. B. Reese, "The thermal decomposition of some polyurethane foams," *British Polymer Journal*, vol. 8, no. 2, pp. 48–53, 1976.

[75] J. Li, A. Kazakov, and F. L. Dryer, "Experimental and numerical studies of ethanol decomposition reactions," *The Journal of Physical Chemistry A*, vol. 108, no. 38, pp. 7671–7680, 2004.

[76] P. Moravec, J. Smolík, H. Keskinen, J. Mäkelä, and V. Levdansky, "Vapor Phase Synthesis of Zirconia Fine Particles from Zirconium Tetra-Tert-Butoxide," *Aerosol and Air Quality Research*, vol. 7, pp. 563–577, 2007.

[77] A. Radtke, P. Piszczek, T. Muziol, A. Wojtczak, and A. Grodzicki, "Synthesis, structural characterization, and thermal properties of zirconium(IV) β-ketodiester complexes," *Structural Chemistry*, vol. 21, pp. 367–375, 2009.

[78] L. Weng, X. Bao, and K. Sagoe-Crentsil, "Effect of acetylacetone on the preparation of PZT materials in sol–gel processing," *Materials Science and Engineering: B*, vol. 96, no. 3, pp. 307–312, 2002.

[79] D. Wyrzykowski, E. Hebanowska, G. Nowak-Wiczk, M. Makowski, and L. Chmurzyński, "Thermal behaviour of citric acid and isomeric aconitic acids," *Journal of Thermal Analysis and Calorimetry*, vol. 104, no. 2, pp. 731–735, 2011.

[80] H. Zhang, C. Tang, Y. Lv et al., "Synthesis, characterization, and catalytic performance of copper-containing SBA-15 in the phenol hydroxylation," *Journal of Colloid and Interface Science*, vol. 380, no. 1, pp. 16–24, 2012.

[81] J. A. Cecilia, R. Moreno Tost, and M. Retuerto Millán, "Mesoporous materials: from synthesis to applications," *International Journal of Molecular Sciences*, vol. 20, no. 13, p. 3213, 2019.

[82] D. Hanaor and C. Sorrell, "Review of the anatase to rutile phase transformation," *Journal of Materials Science*, vol. 46, no. 4, pp. 855–874, 2011.

[83] O. Kurapova and V. G. Konakov, "A Corriger Dans le Texte Aussi Oy Kurapova, and VG Konakov," *Reviews on Advanced Materials Science*, vol. 36, pp. 177–190, 2014.

[84] F. H. Brown Jr. and P. Duwez, "The zirconia-titania system," *Journal of the American Ceramic Society*, vol. 37, no. 3, pp. 129–132, 1954.

[85] J. Yang and J. M. F. Ferreira, "Inhibitory effect of the Al2O3–SiO2 mixed additives on the anatase–rutile phase transformation," *Materials Letters*, vol. 36, no. 5-6, pp. 320–324, 1998.

[86] A. Kubiak, K. Siwińska-Ciesielczyk, and T. Jesionowski, "Titania-based hybrid materials with ZnO, ZrO2 and MoS2: a review," *Materials*, vol. 11, no. 11, p. 2295, 2018.

[87] S. Mascotto, D. Wallacher, A. Brandt et al., "Analysis of microporosity in ordered mesoporous hierarchically structured silica by combining physisorption with in situ small-angle scattering (SAXS and SANS)," *Langmuir*, vol. 25, no. 21, pp. 12670–12681, 2009.

[88] M. Impéror-Clerc, P. Davidson, and A. Davidson, "Existence of a Microporous Corona around the Mesopores of Silica-Based SBA-15 Materials Templated by Triblock Copolymers," *Journal of the American Chemical Society*, vol. 122, pp. 11925–11933, 2000.

[89] S. Fessi, A.-S. Mamede, A. Ghorbel, and A. Rives, "Sol–gel synthesis combined with solid–solid exchange method, a new alternative process to prepare improved Pd/SiO2–Al2O3 catalysts for methane combustion," *Catalysis Communications*, vol. 27, pp. 109–113, 2012.

[90] T. Hirai, H. Sato, and I. Komasawa, "Mechanism of formation of titanium dioxide ultrafine particles in reverse micelles by hydrolysis of titanium tetrabutoxide," *Industrial and Engineering Chemistry Research*, vol. 32, no. 12, pp. 3014–3019, 1993.

[91] H. Kumazawa, Y. Hori, and E. Sada, "Synthesis of spherical zirconia fine particles by controlled hydrolysis of zirconium tetrabutoxide in 1-propanol," *The Chemical Engineering Journal*, vol. 51, no. 3, pp. 129–133, 1993.

[92] S. G. Kumar and K. S. R. K. Rao, "Polymorphic phase transition among the titania crystal structures using a solution-based approach: from precursor chemistry to nucleation process," *Nanoscale*, vol. 6, no. 20, pp. 11574–11632, 2014.

[93] D. R. Dunphy, P. H. Sheth, F. L. Garcia, and C. J. Brinker, "Enlarged Pore Size in Mesoporous Silica Films Templated by Pluronic F127: Use of Poloxamer Mixtures and Increased Template/SiO_2 Ratios in Materials Synthesized by Evaporation-Induced Self-Assembly," *Chemistry of Materials*, vol. 27, pp. 75–84, 2014.